Feasibility of fully automated detection of fiducial markers implanted into the prostate

Harris EJ, McNair HA, Evans PM

1. Introduction

Inaccurate patient set up and tumour movement will lead to errors in the targeting of dose deposition in conformal radiotherapy. In general, to reduce the effects of set-up errors position verification is performed using electronic portal imaging devices (EPIDs) prior to treatment. Because the prostate cannot normally be visualised with megavoltage portal imaging, conventionally, for prostate radiotherapy patients position set-up errors have been determined by matching the position of the bony anatomy in the portal image to that in digitally reconstructed radiographs (DRRs). Increasingly commonplace now is the use of fiducial markers implanted into the prostate.[1] Made from high-density and high atomic number material, such as gold, markers are more radio-opaque than soft tissue providing greater image contrast and are therefore more visible in portal images. The 3D position coordinates of each marker can be found from two portal images acquired at two different angles. By using the coordinates of the centre of mass of 3 or more fiducial markers the position of the prostate can be more accurately identified. However in lateral views, markers are often not clearly visible especially in the presence of highly attenuating patient anatomy such as the femoral heads and the pelvis. In this case, a-priory knowledge of the marker position at the time of the planning CT can assist and commonly this is in the form of the DRRs in which markers are more readily visualised. Automatic detection of fiducial markers will simplify marker identification; removing the need for radiographers to "match" the portal image to the DRR and therefore speeding up the position verification process. Tumour movement during treatment (intrafraction motion) is another potential source of error in dose delivery. Fiducial markers can be used to identify changes in prostate position using portal images acquired continuously during treatment.[2] This enables the treatment to the "gated" i.e. the treatment can be stopped when the prostate moves out of a predetermined treatment space. To determine where the prostate is in real-time will also require some method of automatically detecting the position of fiducial markers.

A number of authors have presented different methods for the automatic detection of markers implanted in the prostate, using EPIDs. Balter et al.[3] (1993) were the first group to address the technical feasibility of automated localisation of the prostate. Using a reference image acquired on the first day of treatment, Balter et al. demonstrated the automatic detection of markers implanted in both humanoid phantom and patients. Later Nederveen et al.[4,5] (2000, 2001) measured detection success rates and localisation accuracy using an automatic detection algorithm based upon a rectangular Marker Extraction Kernel (MEK) specifically designed to mimic the appearance of cylindrical fiducial markers. A similar approach was adopted by Buck et al.[6] (2003) who used a Mexican hat filter (MHF) to identify spherical markers. Also in 2003 Aubin et al.[7] described an automatic detection algorithm that uses a series of steps to enhance portal images and identify marker locations that are initially determined from points of maximum attenuation. Locations are verified

through the application of image filters or templates and by constellation analysis that uses the spatial relationship between markers. Table 1. summarises the study parameters for each of the published studies. The greater challenge for portal imaging is the lateral (LAT) views and therefore percentage detection success rates published by the authors for lateral views are also presented in table with the exception of Buck et al. who considered anterior (AP) views only. Direct comparison of these methods and the reported detection success rates is problematic due to variation of the study parameters. For example Nederveen et al. report 99% detection rate for 1.2mm diameter markers, however markers were not inserted into the prostate but placed on the patients skin at beam exit. Due to x-ray imaging geometry, placing the markers at beam exit (closer to the EPID) will make them appear smaller in the image and therefore arguably more difficult to detect then those positioned inside the prostate. However by placing the markers at the skin exit they will attenuate scatter from the patient and the markers will have greater image contrast which improves the probability of detection. Clearly making a comparison of detection efficiencies for markers placed at different positions is not straightforward. Similarly for the methods of Aubin and Balter who employ markers that are close in size comparison is difficult as they use different EPIDs and different exposures (number of MUs).

In this paper we make a direct comparison of the techniques described above by implementing each method for the detection of markers in portal images acquired of prostate radiotherapy patients that have had fiducial markers implanted in the prostate. By performing the marker detection on the same images we have determined which method gives the highest detection success rates for our images enabling a side-by-side comparison. In addition we compare detection success rates for lower exposure set-up portal images and treatment time images. Each of these techniques requires some level of a-priory knowledge obtained either at the time of planning or from the portal images themselves. The amount of a-priory information used and how it effects how the techniques are implemented, is discussed.

	Balter (1995)	Nederveen (2001)	Buck (2003)	Aubin (2003)
Marker size	1.6mm ∅ sphere (Au)	1.2 mm∅ x 5mm (Au) 1.0 mm∅ x 5mm (Au) 1.0 mm∅ x 10mm (Au)	1.0mm ∅ sphere (W) 1.5mm ∅ sphere (W) 2.0mm ∅ sphere (W)	1.6 mm∅ x 2.6mm (Au)
Marker location	prostate	skin (beam exit)	skin (beam entry)	prostate
No. patients/lateral image	2/18	15/300	12/0	7/308
EPID	Theraview	a-Si flat panel (Heimann)	IView^{GT}	BeamView^{Plus}
Exposure (MU)	4 (6MV) 15 (15MV)	1.5 (18MV) open	3-5 (15MV)	75
Detection success rate % (LAT)	88	99 90 95	AP only 95 99	80

Table 1. Summary of study parameters and detection efficiencies for the four different methods of automatic detection of fiducial markers implanted into the prostate that will be compared.

2. Materials and methods

2.1 Image Acquisition

Prior to planning CT and treatment simulation consenting patients had 3 gold markers implanted into their prostate under transrectal ultrasound guidance. These patients were part of an initial study designed to assess the efficacy of fiducial markers for the assistance of patient position verification and the measurement interfractional and intrafractional prostate motion. The markers are 8mm in length and have a 1mm diameter. A marker diameter of 1mm can be inserted using the standard biopsy needle used for prostate biopsy and was chosen to minimise patient discomfort whilst the length of 8mm was chosen to increase marker visibility. Both gold markers and bony anatomy were outlined on DRRs at the time of treatment planning. Portal set up images were acquired prior to treatment on the first five days of treatment and once a week thereafter. Images were acquired for each field using 1MU, 6MV and the field size was selected to include the bony anatomy for matching. Both AP and lateral projections were acquired. In addition to set up images, "movie" images were also acquired during treatment. The movie image acquisition software automatically sums 8 frames of data and saves this as one image. This corresponds to approximately 7.6MU for a 200MU/min treatment dose rate. All images were acquired with an a-Si EPID (*iview*^{GT} Elekta Oncology Systems, Crawley, UK). For this study, the image sets including the DRRs from 7 patients were used and included: 75 AP and 69 LAT set-up images and 51 AP and 83 LAT movie images. Lateral movie images obtained during treatment included a XX° wedge.

2.2 Marker detection

The different marker detection methods that will be compared are described in the in the literature.[3-7] Each of the methods have been implemented following these descriptions however in order to make greater use of the a-priory knowledge available and to make a fairer comparison of the techniques some steps have been added. These changes, and for completeness, brief descriptions of the methods, are given below.

2.2.1 A-priory knowledge

A-priory knowledge about the markers can be used to improve the accuracy and speed of the detection methods. For this study, this knowledge was obtained from the DRRs generated at the time of treatment planning and includes:

position with respect to the isocentre
length
width
orientation
and inter-marker distances

All values are projected to the imaging plane. To extract this information for each marker cross-sectional DRR image profiles were obtained perpendicular and parallel to the marker length. Marker dimensions were found by differentiating the profiles and finding the minima which correspond to the edge of the marker. Using these minima, marker co-ordinates (in pixel units relative to the isocentre) of the centre and ends of the marker were found and used to calculate the length, width and orientation of the markers. The pixel resolution of the DRR differed to that of the portal images and therefore these co-ordinates had to be re-scaled using the ratio of the pixel/mm in the DRR to that of the portal image. Due to a small positional error on the portal imager, which includes the effect of detector sag, the projection of the isocentre did not always coincide the centre of the portal imager. The projection of the isocentre was identified by finding the field edges and using these as a reference to calculate its position. The position with respect to the isocentre, size and orientation of the markers as they appear in the portal could then be predicted.

2.2.2 Template matching

Both of the techniques described by Nederveen and Buck are based on template matching image processing techniques[9]. Marker locations can be found by convolving the portal image with a digitally constructed template that has been chosen to mimic the projection of the fiducial marker. The image coordinates of the pixel with highest intensity in the resultant image corresponds to the marker position. Nederveen et al.[4] have presented a marker extraction kernel (MEK) to be used as a template. This template is illustrated in figure 1 and is represented by three rectangular regions, L_{ab}, L_{ε} and L_{δ}. The region dimensions (in pixels) are given by parameters a, b, ε and δ.

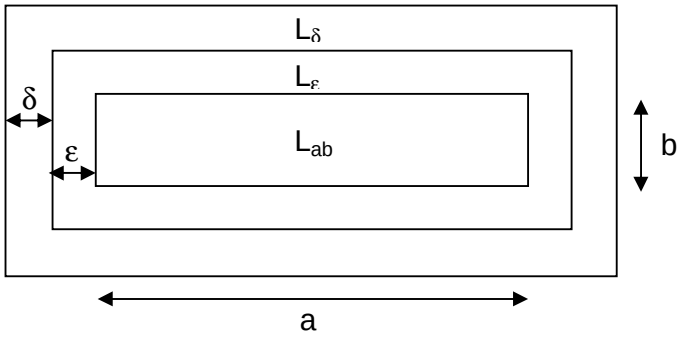

Figure 1. Marker extraction kernel that consists of a central region L_{ab} and two borders L_{ε} and L_{δ}.

Because markers are cylindrical their rotational asymmetry means that marker projections will have varying width, length and orientation. For this study parameters a and b were found for each marker in both LAT and AP views using the DRRs. Parameters ε and δ were kept constant. Each region of the kernel is weighted using a weight parameter *w*. In ref. 5 Nederveen describes a method for calculating a weighting function which compares the second derivative of a function that mimics the shape of the marker to marker images. Again because the markers are cylindrical

the weighting function can be expected to change with the orientation of the marker. The weighting function therefore has to be derived from portal images of markers at each orientation or some "average" weighting function must be chosen to represent the marker at all orientations. Note that this weighting function cannot be obtained from the DRR as the pixel resolution of the DRR is inadequate to describe the spatial variation of intensity at the marker edges. Nederveen notes in ref. 5 that the weights used for their MEK are comparable to the integer weights given in ref 4 and therefore these weights were used. Generating a template with the weights recommended in ref 4. produces the template shown in figure 2a. The weights of the MEK means that the convolution of the image with the template shown in figure 2a produces a marker value (MV) which gives maximal response when the MEK is centred on a marker-like shape.

Buck et al. propose a cylindrical Mexican hat filter (MHF) for the detection of cylindrical markers based on the second derivative of the 2D Gaussian which has different widths for x and y directions and is fitted to:

$$\psi_c^{(2)}(x,y,a,b) = \frac{1}{ab}\left(1-\frac{x^2}{a^2}+\frac{y^2}{b^2}\right)e^{-\left[\frac{x^2}{2a^2}+\frac{y^2}{2b^2}\right]}$$

Marker templates were created using values of a and b that represent the dimensions of the marker projection in the x- and y-directions respectively; again values were acquired from the DRRs. An example of the MHF template (a = 10, b = 4) is shown in figure 2b. This shows the negative lobes characteristic of the second derivative. The negative values in both of these templates make them more sensitive to objects that are the same size as the marker. Without these negative values uniform areas of high intensity will give greater values when convolved with the template.

Both MEK and MHF templates were rotated to match the orientation of the markers at the time of planning CT. Search areas of 64 x 64 pixels centred on predicted marker locations obtained using the DRR were defined. Projected to the plane of the isocentre 64 pixels is equivalent to approximately16mm which is twice the expected maximum distance which the prostate will move.[3] MEK and MHF maker templates were simply convolved with the search area and the pixel with the maximum intensity in the resultant image corresponds to the marker location. Because the markers are able to rotate within the patient, marker templates were rotated in steps of 5 degrees through + 20 to - 20 degrees from their original orientation prior to being applied. The greatest MV or highest intensity corresponds to the detected marker orientation.

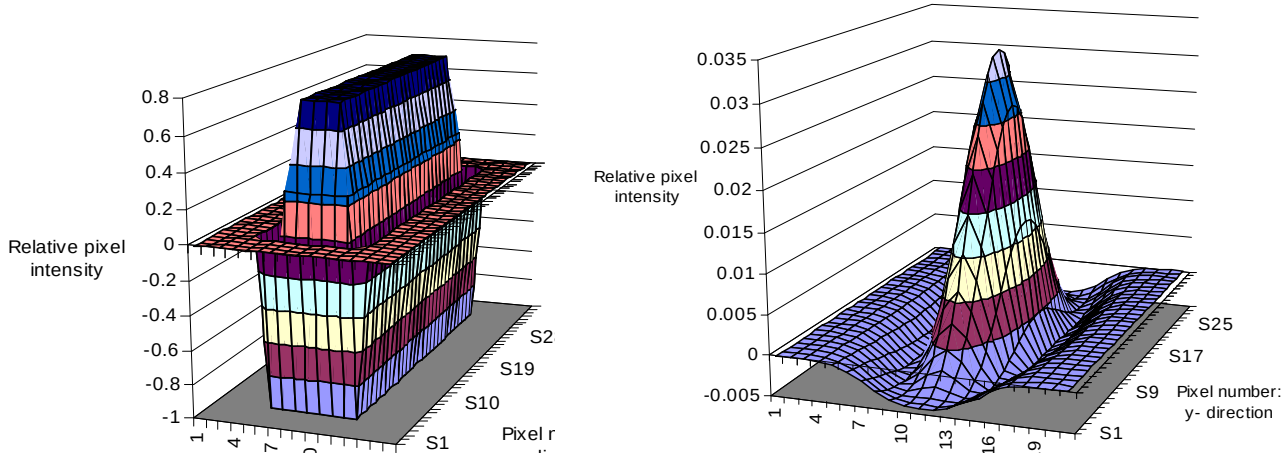

Figure 2. Templates used to detect fiducial markers a) Marker Extraction Kernel with weighting function applied described by Nederveen et al. (2000) and b) Mexican Hat Filter used by Buck et al. (2003).

2.2.3 Attenuation and constellation analysis

Aubin et al. have presented an algorithm based on the identification of image intensity minima which represent regions of maximum attenuation. Verification of minima as potential marker positions is preformed using templates to create a contrast image and the distance between markers to increase the detection probability. A complete description of the six steps followed to implement the algorithm is given by Pouliot et al.[8] The six steps, were followed with the exception of changes made to step three and the exclusion of step six, are now briefly summarised: (1) definition of search area (as for template matching described above), (2) image filtering to reduce noise (3 x 3 averaging filter) and contrast enhancement (contrast limited histogram equalisation), (3) a contrast image is formed and local minima positions identified, (4) the intensity of the minima is found, (5) minima are grouped together based on the inter-marker distances obtained from the DRR, the combined maximum intensity for a group gives the most probable marker positions and (6) marker validation by neural network. Because Aubin et al. describe an algorithm suitable for spherical markers changes to step three had to be made to optimise the method for cylindrical markers. In step three, Aubin separately convolves unit ring and unit circle templates with the search area image and divides the resulting convolved circle image by the ring image to create a "contrast" image. This mimics the effect of the negative values in the templates employed by Buck and Nedreveen giving larger values where marker shapes are found. For this study, elliptical templates were employed, the size, shape and orientation of the ellipses were varied according to the size and orientation of the marker projection in the DRR. Once step five is complete the most probable marker positions have been identified: this is the final stage for both the template matching and cross correlations methods. Step six described by Pouliot is used only to validate the marker selection and categorise whether the marker detection was true or false, therefore this stage was omitted from the analysis.

2.2.4 Cross correlation

Normalised cross-correlation can be used to find the similarity between two images.[9] This method requires the greatest level of a-priory knowledge in that it uses a reference image of the marker selected from a portal image to carry out the search. Balter et al.[3] proposed using portal images obtained on the first day of treatment to create marker reference images that can then be cross-correlated with images obtained on subsequent treatment days. To implement this method, marker positions were manually identified from treatment time portal images acquired on the first day of treatment. Marker reference images used for the search were then obtained by selecting a region of interest around the marker location. As described above a search area was defined in all subsequent images using the information from the DRRs. A

uniform 2×2 averaging filter was applied to the reference image and the portal image to remove high frequency noise. A normalised cross-correlation was then performed for each marker at each pixel position within the search area. The marker position corresponds to the pixel with the highest correlation value.

2.2.5 Localisation accuracy

To access detection success rate marker positions found with each of the methods need to be compared with actual marker positions. Actual marker positions were determined by manually identifying the two ends of the markers in the portal image and calculating the mid-marker co-ordinates. Uncertainties introduced by the manual identification were reduced by the identification of marker locations three times in three different sittings. In general, marker positions were difficult to identify in the lateral images which resulted in a greater inaccuracy. To assess the uncertainty in the position accuracy, the average standard deviation (S.D.) in marker position was found by locating 6 markers in lateral images 10 times. For anterior images, marker locations obtained by the algorithms described above were considered to be correct if they were within ± 4 pixels (in both x and y directions) of the actual marker position. This corresponds to a ± 1mm tolerance. This was increased to ± 4 pixels + S.D. (± 6 pixels) for lateral images. The detection efficiency is defined the fraction of marker positions that fall within this tolerance.

3. Results

3.1 Detection success rate

Table 2. compares the percentage detection success rates for the four automatic marker detection methods described above. Detections rates are given separately for anterior and lateral images for both set up (1MU) and treatment-time images (7.6 MU).

	1MU		7.6MU	
Method	Anterior	Lateral	Anterior	Lateral (wedge)
Template (Nederveen et al.)	75	37	93	58
Template (Buck et al.)	72	35	90	59
Attenuation analysis	91	42	96	67
Cross correlation	99	83	100	99

Table 2. Percentage detection success rates for the four automatic marker detection methods compared in this study.

3.2 Localisation confidence

A marker detection success is defined as a marker fond within 1mm or 1mm + 0.5mm of the actual marker location for AP and LAT images respectively. However when the actual marker location is unknown and in the absence of a method with 100% detection efficiency it will be advantageous to have some measure of confidence in the marker position returned by the automatic method. Both the template matching method and the cross correlation methods rely on some peak value to identify the position of the marker. In the template matching case the peak value can be normalised in order to compare marker values for different markers and across subsequent images. This was achieved by dividing the maximum intensity value by the average intensity in the search area and the maximum possible marker value for a given MEK or MHF. The correlation coefficient (CC) is normalised to produce a correlation value between 1 and 0 with maximum correlation being 1. Average MV and CC for markers that have been successfully detected and those that have not are compared in table 3.

	Marker values		Correlation coefficient	
	Detected	Not detected	Detected	Not detected
Anterior (1MU)	0.25	0.26	0.78	0.69
Lateral (1MU)	0.095	0.09	0.65	0.68
Anterior (8MU)	0.29	-	0.8	-
Lateral (8MU)	0.15	0.155	0.85	-

Table 3. Average marker values and correlation coefficients for detected and non-detected markers.

4. Discussion and conclusions

The results in table 2 show that the detection success rates for all methods increase for images taken with a higher number of monitor units. This is expected because increased dose results in greater signal to noise ratio enabling fiducial markers to be visualised more easily. If we compare the detection success rates for all four methods it is evident that the two template matching methods give similar results which is also unsurprising as the templates share similar characteristics, i.e. their shape and negative lobes to pick out cylindrical shapes, and are used in the same manner. Both template matching methods produced poorer results compared to those presented in the literature. As previously discussed Nedreveen et al. placed markers at the beam exit which results in an increase in contrast of the markers due to the absence of scatter from the patient below the marker plane making markers easier to identify. The higher detection success rates of markers in AP views using the MHF filter presented by Buck et al. could also be due to marker location. Markers were placed at the beam entry which would magnify the markers in the image however there would be a reduction in marker contrast due to increase scatter occurring inside the patient

past the marker plane. Buck et al. also used greater diameter markers and a higher number of MUs which is a more likely explanation of their higher detection rates.
In all cases the cross correlation method produces the highest detection success rates. Comparison of detection success rates published for attenuation analysis compared to those obtained in this study is difficult because of the greatly different image acquisition parameters. Detections rates for the cross correlation method are similar however Balter published results for only two patients.

Analysis of the marker positions given by the four methods shows that for anterior images marker detection failure for template matching is almost always due to the fact that the method has found one marker in preference to another. This is avoided in the attenuation analysis method where all three marker positions are considered at once using the inter-marker distances hence the detection efficiency is higher. For template matching, this error could be reduced by making the search area smaller however this could result in higher detection failures as the markers would then be more likely to move outside of the search area. Another option is to increase inter-marker distances at the time of insertion however this may not always be practicable and could not be relied upon. Detection failures for the attenuation analysis tend to occur due to the misidentification of regional minima using inter-marker distances where minima from bony anatomy are situated close to marker minima. The cross correlation method uses a reference image that may include more than one marker if they are in close proximity and thus includes information about the background to a specific marker helping to distinguish between markers. For lateral images errors are due to poor image contrast and the fact that in many cases the bony anatomy obscures marker shape. This problem is more significant for template matching and attenuation analysis that rely on the likeness of a set marker shape.

The cross correlation method relies upon the greatest level of a-priory knowledge, an image of the marker in-vivo. Therefore this method requires manual intervention on the first day of radiotherapy treatment and cannot be considered fully automated. The requirement for intervention at the time of the first fraction is also discussed by Nederveen et al. who discuss the need for a manual check of the accurate detection of markers at the time of the first fraction. This is to ensure that all three markers are present and are not obscured by bony anatomy. Considering this requirement there is no obvious disadvantage of the cross-correlation method.

The results presented in table 3 show there is no significant difference between MVs or CCs for successfully and unsuccessfully detected markers. This is in agreement with the analysis of the marker location failures for anterior images for which a marker detection failure is most likely due to the detection of another marker. For lateral images poor image contrast and high noise means that correlation values are low even in the case of accurate location giving poor detection confidence. Therefore, the MV or CC cannot be used to indicate the confidence with which the marker location has been identified. Because CCs do not provide a measure of confidence means that it is not possible to alert the radiographer to any possible failures in the detection method.

For unsupervised fully automated patient set-up we require 100% detection efficiency. The results for set up images indicate that none of these methods will provide this for our current imaging protocol. For 1MU images, the highest detection

success rate is obtained with the cross correlation method (83%). This is problematic, especially in view of the fact that the method will always supply an answer and we have no measure of the confidence with which a particular marker is identified. However, detection success rates of 99% can be achieved with an almost eightfold increase in dose. Clearly these doses are too high to be used for purely imaging purposes however with the inclusion of markers there is scope to use a fraction of the treatment dose by employing the same fields as the treatment. The same arguments apply for intrafraction imaging, an increase in image dose will enable high detection success rates to be achieved. In contrast however, for portal imaging to be used to monitor prostate position during treatment, images must be obtained at suitably regular intervals. For lateral treatment fields, the dose per field is on the order of 150-200 MU and therefore 7.6MU represents approximately 5% of the dose delivered. This means that potentially 5% of the dose could be delivered with the prostate outside of the treatment space before the error is detected. A trade off between detection success rate and the potential fraction of incorrectly delivered dose therefore exists. Further work is required to identify the minimum dose required to obtain 100% detection success rate.

In conclusion we have directly compared four methods for the automatic detection of fiducial markers that have been implanted into the prostate. This work has shown that a fully automated method of marker detection for the first day of treatment is unachievable using these methods and that using cross-correlation is the best technique for automatic detection on subsequent radiotherapy treatment days.

References

1. P. J. Keall, A. D. Todor, S. S. Vedam et al., "On the use of EPID-based implanted marker tracking for 4D radiotherapy", *Med. Phys.* Vol. **31** No.12, pp. 3492-3499, 2004.
2. S. Shimizu, H. Shirato, K. Kitmura et al. "Use of an implanted marker and real-time tracking of the marker for the positioning of prostate and bladder cancers", *Int. J. Radiation Oncology Biol. Phys.*, Vol. **48**, No. 5, pp. 1591–1597, 2000.
3. J. Balter et al., "Automated localisation of the prostate at the time of treatment using implanted radiopaque markers", *Int. J. Radiation Oncology Biol. Phys*., Vol. **38**, No. 5, pp. 1281–1286, 1995.
4. A. J. Nederveen, J. J. W. Lagendijk and P Hofman,"Detection of fiducial gold markers for automatic on-line megavoltage position verification using a marker extraction kernel (MEK)", *Int. J. Radiation Oncology Biol. Phys*., Vol. **47**, No. 5, pp. 1435–1442, 2000.
5. A. J. Nederveen, J. J. W. Lagendijk and P Hofman, "Feasibility of automatic marker detection with an a-Si flat-panel imager", *Phys. Med. Biol*. Vol. **46,** pp. 1219 – 1230, 2001.
6. D Buck, M Alber and F Nusslin, "Potential and limitations of the automatic detection of fiducial markers using an amorphous silicon flat-panel imager", *Phys. Med. Biol*. Vol. **48,** pp. 763 - 764, 2003.

7. S. Aubin et al., “Robustness and precision of an automatic marker detection algorithm for online prostate daily targeting using a standard V-EPID”, *Med. Phys.* Vol. **30** No.7, pp. 1825-1833, 2003.
8. S. Pouliot, A. Zaccararin, D. Laurendeau and J. Pouliot, “Automatic detection of three radio-opaque markers for prostate targeting using EPID during external radiation therapy”, International conference on image processing (ICIP), pp. 857 – 860, 2001.
9. R. C. Gonzalez and R. E. Woods, “Digital Image Processing”, Wiley, New York, 1978.